

# ViewMorpher3D: A 3D-aware Diffusion Framework for Multi-Camera Novel View Synthesis in Autonomous Driving

Farhad G. Zanjani Hong Cai Amirhossein Habibian

Qualcomm AI Research\*

{fzanjani, hongcai, ahabibia}@qti.qualcomm.com

## Abstract

Autonomous driving systems rely heavily on multi-view images to ensure accurate perception and robust decision-making. To effectively develop and evaluate perception stacks and planning algorithms, realistic closed-loop simulators are indispensable. While 3D reconstruction techniques such as Gaussian Splatting offer promising avenues for simulator construction, the rendered novel views often exhibit artifacts, particularly in extrapolated perspectives or when available observations are sparse.

We introduce *ViewMorpher3D*, a multi-view image enhancement framework based on image diffusion models, designed to elevate photorealism and multi-view coherence in driving scenes. Unlike single-view approaches, *ViewMorpher3D* jointly processes a set of rendered views conditioned on camera poses, 3D geometric priors, and temporally adjacent or spatially overlapping reference views. This enables the model to infer missing details, suppress rendering artifacts, and enforce cross-view consistency.

Our framework accommodates variable numbers of cameras and flexible reference/target view configurations, making it adaptable to diverse sensor setups. Experiments on real-world driving datasets demonstrate substantial improvements in image quality metrics, effectively reducing artifacts while preserving geometric fidelity. <https://qualcomm-ai-research.github.io/viewmorpher3d>

## 1. Introduction

Novel-view synthesis (NVS) has advanced rapidly with neural scene representations such as Neural Radiance Fields (NeRF) [16] and 3D Gaussian Splatting (3DGS) [11]. Yet, even state-of-the-art 3DGS reconstructions degrade under sparse observations, wide-baseline extrapolation, or dynamic content, producing floaters, texture bleeding,

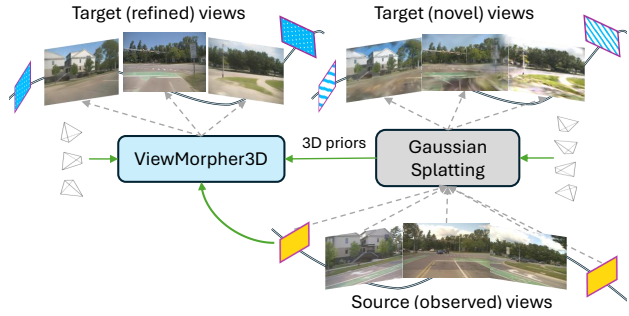


Figure 1. *ViewMorpher3D* improves rendered novel views via multi-view diffusion, conditioned on camera images, poses, and the scene’s 3D structure.

and hollow structures that propagate into rendered views. Diffusion-based enhancement has recently emerged as a compelling remedy: by leveraging powerful image priors, one can repair underconstrained regions and recover perceptual detail without re-optimizing the underlying 3D representation. However, existing enhancers are typically driven by RGB renderings from the current 3D model and treat geometry only implicitly, particularly when the rendering is most unreliable. When artifacts overwhelm the RGB signal, the denoiser can be misled, yielding visually pleasing but structurally implausible results or multi-view inconsistencies.

Prior efforts fall along three axes. Geometry-regularized reconstruction methods [25] add depth/normal constraints to the 3D optimization, strengthening geometry but remaining sensitive to noise and view sparsity. Methods that inject generative priors into optimization—e.g., RegNeRF [19] and VEGS [9]—can hallucinate plausible appearance for unseen regions, yet they commonly rely on single-view supervision or static priors and thus struggle to guarantee multi-view and temporal coherence. Most relevant to our setting are diffusion-based enhancers that operate at

\*Qualcomm AI Research is an initiative of Qualcomm Technologies, Inc.

the image level: DiFix3D+ [24] employs a single-step latent diffusion model to clean rendered views (with optional reference-image conditioning), and 3DGS-Enhancer [14] leverages a video diffusion prior to promote consistency over time. While effective, these approaches predominantly condition on RGB renders and fixed (or narrow) input layouts; as a result, they remain brittle when the rendered inputs are severely corrupted and do not natively scale to variable numbers of cameras and time steps.

We address these limitations with *ViewMorpher3D*, a diffusion-based enhancer purposely built for Gaussian-splatting NVS that is both geometry-aware and view/time scalable. At its core is a new architecture that *jointly* processes a *variable-cardinality* set of inputs drawn from heterogeneous cameras and time steps, and that produces a variable number of enhanced target views. The model aggregates evidence through a permutation-invariant fusion of latent features, enabling cross-view context to flow not only from reference images to targets but also *among* targets, which improves spatial consistency in multi-camera settings and temporal coherence in sequential ones. Crucially, rather than relying on RGB renders alone, we introduce a *geometrical conditioning* interface that exposes the denoiser to 3D-aware signals derived from the current 3DGS scene and camera poses. Concretely, we condition on rendered coordinate maps (which convey pixel-aligned 3D correspondences) and pose-aware embeddings (e.g., Plücker ray fields). These signals inform the diffusion process about where the structure is supported, uncertain, or contradictory between views, enabling the model to suppress floating particles, respect occlusions, and recover high-frequency detail *without* sacrificing geometric plausibility.

Our formulation treats multi-view enhancement as conditional image restoration in the latent space of a distilled diffusion model. To make joint enhancement efficient at scale, we supervise all targets at the latent level while decoding and supervising only a sampled subset of images per iteration, which amortizes memory without weakening cross-view coupling. The result is a flexible enhancer that (i) accepts and benefits from more views when available but remains effective in the low-signal regime, (ii) improves perceptual quality and view consistency over RGB-only enhancers such as DiFix3D+ [24], and (iii) achieves stronger structural faithfulness than video-prior formulations such as 3DGS-Enhancer [14] when extrapolation and artifacts are severe. The contributions of this work include the following.

- We introduce a conditioning interface that goes beyond RGB renders by injecting 3D correspondence maps and pose-aware embeddings into the denoiser. This grounding markedly improves robustness when rendered inputs are heavily corrupted, reducing hallucinations that violate scene structure.

- We propose a view- and time-agnostic architecture that jointly processes a *variable* number of inputs (across cameras and time) and enhances a *variable* number of targets, enabling content propagation *among* targets and delivering strong cross-view and temporal coherence.
- We couple latent-level supervision for all targets with selective pixel-space supervision, supporting scalable multi-target enhancement without prohibitive memory, and retaining compatibility as a drop-in post-process for 3DGS pipelines.
- Across sparse and extrapolated settings, our method consistently improves image quality and geometric plausibility over the state-of-the-art, including DiFix3D+ [24] and 3DGS-Enhancer [14].

## 2. Related Work

**Neural Rendering and Sparse-View Limitations.** Neural scene representations *e.g.* NeRF [16] and 3D Gaussian Splatting [11] have enabled high-quality novel-view synthesis in static, densely sampled scenes. However, their performance degrades under sparse observations, wide-baseline extrapolation, or dynamic content—common in real-world driving scenarios—leading to artifacts like floaters and texture bleeding. Extensions to driving scenes [5, 27, 29, 31, 33] have improved realism but remain limited to interpolated views or fixed camera layouts.

**Generative Priors in 3D Optimization.** To mitigate reconstruction artifacts, several methods integrate generative priors into the optimization process. RegNeRF [19] and DietNeRF [10] use semantic or photometric regularization to guide appearance synthesis. ReconFusion [26] and VEGS [9] leverage learned generative models to extrapolate unseen content and improve view synthesis quality. VEGS, in particular, distills diffusion priors into 3DGS for urban extrapolation. Despite improved fidelity, these approaches often lack robustness under severe degradation and struggle to enforce multi-view or temporal coherence.

**Diffusion-Based Enhancement.** Recent work reframes NVS enhancement as image-level restoration using diffusion models. DiFix3D+ [24] applies latent diffusion to clean rendered views, but its reliance on RGB inputs limits effectiveness when geometry is unreliable. DiFix++ [20] refines this approach with improved losses. 3DGS-Enhancer [14] defines the task as enhancement of a rendered image sequence between two high quality reference views. The authors introduce a video diffusion prior for temporal consistency, yet its single-camera design and sequential requirements restrict scalability to multi-view settings.

This work presents a latent-space enhancer that jointly restores multi-view renderings using a distilled diffusion model. Unlike prior methods, our approach flexibly adapts to varying numbers of cameras and time steps, and incor-

porates explicit geometric conditioning via visibility-aware projections and camera poses. This enables robust enhancement even under severe degradation, improving both perceptual quality and structural consistency.

### 3. Method

This work addresses the challenge of enhancing novel-view synthesis (NVS) outputs generated from a 3D Gaussian Splatting (3DGS) representation. Given a 3DGS model trained on a scene using a set of  $N$  reference images  $\{I_1^r, I_2^r, \dots, I_N^r\}$  and their corresponding camera poses  $\{P_1^r, P_2^r, \dots, P_N^r\}$ —collectively referred to as *reference views*—our objective is to improve the quality of  $M$  low-fidelity rendered images  $\{I_1^t, I_2^t, \dots, I_M^t\}$  associated with novel camera poses  $\{P_1^t, P_2^t, \dots, P_M^t\}$ , referred to as *target views*, produced by the 3DGS model.

We reformulate the challenging problem of 3D-consistent image generation as a task of multi-view conditional image restoration, aiming to recover high-quality target views from distorted renderings. To this end, we propose *ViewMorpher3D*, a diffusion-based enhancement model that leverages reference views, camera poses, and 3D priors to restore missing details and suppress rendering artifacts. By incorporating a learned diffusion prior and conditioning on observed reference data, the model reconstructs degraded regions and infers plausible visual content.

An overview of the ViewMorpher3D pipeline is presented in Fig. 2, which its components detailed in the following subsections.

#### 3.1. Geometric Priors

**Geometric Image Rendering** Beyond RGB rendering—where color values from 3D Gaussian primitives are projected onto the 2D camera plane—we introduce *geometric rendering*, which encodes the 3D coordinates of Gaussian centers instead of colors.

RGB rendering maps color vectors to pixels, whereas geometric rendering projects *3D world coordinates* onto the image plane, producing per-pixel 3D coordinate maps (C-maps). These maps capture spatial correspondences from the camera viewpoint. Although C-maps for target views may be noisy, they provide useful guidance during diffusion-based restoration. Conditioning on C-maps for both reference and target views enables 3D-aware consistency across views.

A *3D coordinate map*  $\mathbf{X}(u, v) \in \mathbb{R}^3$  for pixel  $(u, v)$  represents the estimated 3D world coordinates of the visible surface point, computed by weighted accumulation along the viewing ray:

$$\mathbf{X}(u, v) = \sum_{i=1}^N \alpha_i(u, v) \prod_{j=1}^{i-1} (1 - \alpha_j(u, v)) \cdot \mathbf{x}_i, \quad (1)$$

Here  $(u, v) \in \{1, \dots, H\} \times \{1, \dots, W\}$  are pixel coordinates for an image of size  $H \times W$ .  $\mathbf{x}_i \in \mathbb{R}^3$  is the 3D world coordinate of sample  $i$  (e.g., a point along the ray or Gaussian center), and  $\alpha_i(u, v)$  is its opacity contribution, indicating influence on the final coordinate. This parallels volumetric rendering, where samples are accumulated by visibility and contribution.

For Gaussian Splatting,  $\alpha_i(u, v)$  is the opacity of the  $i^{\text{th}}$  Gaussian projected onto  $(u, v)$ . A similar formulation applies to NeRF-based methods for generating C-maps. Visual examples of rendered C-maps are provided in supplementary materials.

**Camera Representation** To further enhance image restoration, we incorporate camera poses of both reference and target views alongside the rendered C-maps. Following prior work [28], camera poses are encoded using Plücker ray embeddings, which represent pixel-aligned rays as dense 2D image maps. Each ray is defined by a pair  $(\mathbf{o} \times \mathbf{d}, \mathbf{d}) \in \mathbb{R}^6$ , where  $\mathbf{o}$  is the ray origin and  $\mathbf{d}$  is its direction. Prior to computing Plücker ray embeddings, we normalize the pose of cameras. More details on such normalization discussed in the supplementary materials.

#### 3.2. Multi-View Image Diffusion

Inspired by prior works [24], ViewMorpher3D restores rendered images using SD-Turbo [23], a single-step image diffusion model. Given a set of low-quality rendered target frames  $\hat{I}^t$  and relevant reference frames  $I^r$ , we first extract latent features from all frames using a frozen encoder of a pretrained Variational Autoencoder (VAE). The 3D priors are encoded via an auxiliary lightweight encoder and added to the image latents.

The reverse-time Markov chain for a conditional diffusion model is expressed as:

$$p_{\theta}(z_0 \mid \mathbf{c}) = \int p(z_T) \prod_{t=1}^T p_{\theta}(z_{t-1} \mid z_t, \mathbf{c}) dz_{1:T}, \quad (2)$$

where  $z_T \sim \mathcal{N}(0, I)$  is the initial noise sample, and  $p_{\theta}(z_{t-1} \mid z_t, \mathbf{c})$  is the learned reverse conditional transition probability. Instead of starting from noise, we use distorted target views  $\hat{I}^t$  and apply a single-step distilled model that directly approximates the full marginal distribution:

$$p_{\theta}(I^t, \hat{I}^t, I^r, \mathbf{c}) = p_{\theta}(I^t \mid \hat{I}^t, I^r, \mathbf{c}) \cdot p(\hat{I}^t, I^r, \mathbf{c}). \quad (3)$$

The first term in Eq. 3 represents the image-to-image translation probability, parameterized ( $\theta$ ) by a 2D UNet.

The conditioning input  $\mathbf{c} \in \mathbb{R}^{H/8 \times W/8 \times d}$  is a feature vector computed by an auxiliary convolutional encoder  $\Psi$ , which takes as input the prior C-maps  $X$ , Plücker ray embeddings  $P$ , and a binary indicator mask  $M$  distinguishing reference and target views:

$$\mathbf{c} = \Psi(X, P, M). \quad (4)$$

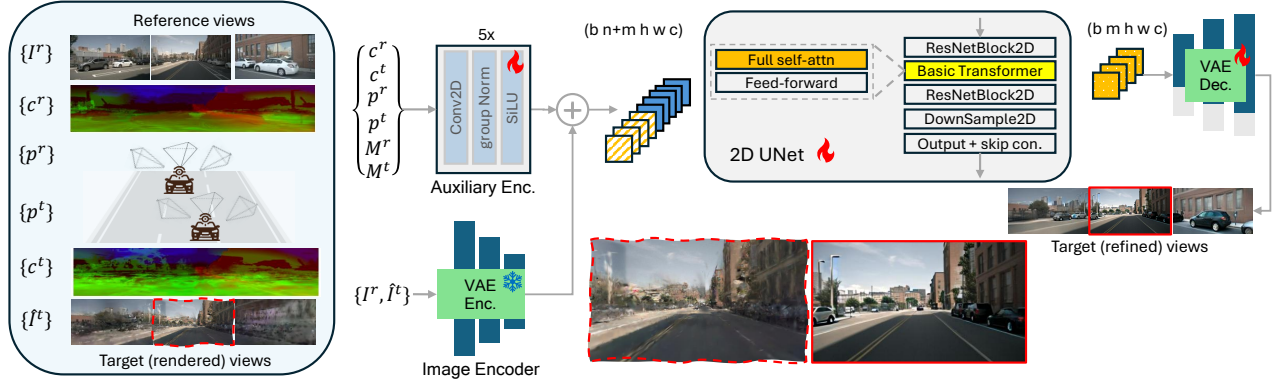


Figure 2. Overview illustration of ViewMorpher3D. The rendered novel-view images are enhanced via a multi-view diffusion model, conditioned on reference views, camera poses and 3D priors.

Condition features are added to the image latents via simple addition, which we show to outperform an alternative cross-attention mechanisms in our ablation study. These condition-added image latents are then stacked and passed to the 2D UNet.

To enforce spatial consistency across reference and target views, ViewMorpher3D applies full 3D self-attention over flattened spatial dimensions. This mechanism captures dependencies across the entire spatial volume of all reference and target views, enabling restoration of missing visual context and ensuring coherence across enhanced views.

**Training Objectives** The learnable parameters of ViewMorpher3D—including the diffusion network and the auxiliary encoder  $\Psi$ —are optimized end-to-end. Unlike prior approaches, we apply supervision at two levels: (i) latent features and (ii) decoded target images. Supervising low-dimensional latent features enables the model to jointly process multiple reference and target views, fostering cross-view consistency. For latent supervision, we adopt the  $v$ -prediction objective [22] with an  $\ell_2$  loss.

Decoding all target views at full resolution during training is computationally prohibitive due to memory constraints. To address this, we employ a partial supervision strategy: at each iteration, only a randomly selected subset of target views is decoded and used for image-level supervision. For these decoded views, we apply a composite loss comprising  $\ell_2$ , SSIM, and LPIPS terms with equal weighting, balancing pixel-level accuracy, structural similarity, and perceptual quality.

Following prior works [21, 24], we further mitigate domain gaps in generation by fine-tuning the VAE decoder using LoRA-based adaptation, jointly with the rest of learning parameters of model. This lightweight approach improves reconstruction fidelity without incurring significant computational overhead.

## 4. Experiments

### 4.1. Datasets

To evaluate the generalization capabilities of NVS methods under challenging conditions of view extrapolation and sparsities, we incorporate four datasets.

**EUVS data** The Extrapolated Urban View Synthesis (EUVS) dataset [7] is a large-scale benchmark designed to assess NVS performance in urban environments where test views significantly deviate from training views. Unlike conventional benchmarks that focus on interpolated views with high spatial correlation, EUVS emphasizes robustness under large viewpoint changes—a critical requirement for vision-centric autonomous driving systems. The dataset comprises 104 real-world urban scenes, captured using multiple vehicles, traversals, and cameras, with designated training and test splits. EUVS includes three evaluation settings: (i) translation, (ii) rotation, and (iii) translation + rotation, which have varying degrees of extrapolation difficulty.

**Para-Lane data** The Para-Lane dataset [18] provides NVS image sequences in multi-lane urban driving scenarios. Similar to EUVS data, it includes parallel driving scans across multiple lanes, enabling evaluation of NVS under cross-lane conditions. The dataset comprises over 16K front-view images and 64K surround-view images, collected via multi-pass trajectories using synchronized multi-sensor setups.

**nuScenes data** To further evaluate NVS methods in realistic autonomous driving scenarios with complex dynamics—including vehicles, riders, and pedestrians—we utilize the nuScenes [3], which contains 750 driving sequences recorded with six cameras in diverse urban environments. Complementing the novel view scenarios in the aforementioned datasets, we partition each video into two consecutive disjoint segments: the frames of the first segment (be-

Method	EUVS Novel-View Data Settings								
	Setting 1			Setting 2			Setting 3		
	PSNR↑	SSIM↑	LPIPS↓	PSNR↑	SSIM↑	LPIPS↓	PSNR↑	SSIM↑	LPIPS↓
3DGS [11]	16.37	0.7203	0.2599	19.53	0.7511	0.2668	14.99	0.7169	0.4050
2DGS [8]	16.30	0.7103	0.2890	18.83	0.7204	0.2917	11.36	0.5447	0.5459
GSPro [6]	16.39	0.7189	0.2450	19.39	0.7470	0.2246	14.82	0.6996	0.3877
PGSR [4]	16.32	0.7102	0.2733	18.38	0.7119	0.2532	14.25	0.6984	0.4363
3DGM [12]	16.35	0.7248	0.2542	18.78	0.7464	0.2813	14.60	0.7233	0.4049
Feature 3DGS [32]	16.01	0.7243	0.2575	19.59	0.7864	0.2278	14.33	0.6386	0.3816
Zip-NeRF [2]	14.06	0.6917	0.3418	17.36	0.6715	0.3582	14.42	0.6565	0.4546
Instant-NGP [17]	12.65	0.6252	0.5938	17.15	0.7212	0.5171	14.39	0.7104	0.6592
VEGS [9]	15.88	0.7047	0.3062	23.33	0.7949	0.2811	14.25	0.6475	0.4422
DIFIX3D [24]	17.09	0.7391	0.2244	20.02	0.7135	0.1871	14.84	0.6655	0.3275
DIFIX3D++ [20]	<b>17.94</b>	0.7821	0.2182	21.68	0.7722	0.2092	15.91	0.7430	0.3351
<b>ViewMorpher3D</b>	17.84	<b>0.7956</b>	<b>0.1922</b>	22.55	<b>0.7957</b>	<b>0.1715</b>	<b>16.60</b>	<b>0.7452</b>	<b>0.2910</b>

Table 1. NVS results on EUVS data across three evaluation settings of view extrapolation. The diffusion enhancers all applied on 3DGS rendered images (appeared with gray color).



Figure 3. Novel-view images of EVUS (left 4 col.) and Para-Lane (right 2 col.) datasets; The qualitative comparison of enhanced 3DGS rendered images from DiFix3D and ViewMorpher3D. The ViewMorpher3D results show a higher fidelity to the scene visual contents.

Method	Single-lane transition			Double-lane transition		
	PSNR↑	SSIM↑	LPIPS↓	PSNR↑	SSIM↑	LPIPS↓
3DGS [11]	17.05	0.524	0.446	16.26	0.505	0.472
2DGS [8]	16.79	0.523	0.469	16.01	0.510	0.494
GSPro [6]	17.01	0.521	0.446	16.29	0.505	0.472
Scaffold-GS [15]	17.59	0.538	0.450	17.09	0.525	0.470
StreetGS [29]	17.50	0.510	0.456	16.16	0.496	0.480
DIFIX3D [24]	17.62	0.470	0.234	16.87	0.447	0.271
DIFIX3D++ [20]	19.25	0.559	0.275	18.55	0.538	0.311
<b>ViewMorpher3D</b>	<b>20.20</b>	<b>0.586</b>	<b>0.208</b>	<b>19.47</b>	<b>0.564</b>	<b>0.233</b>

Table 2. NVS results on Para-Lane data across two extrapolation settings. The diffusion enhancers all applied on 3DGS rendered images (appeared with gray color)

tween 0 and 10 seconds of videos) are used for 3DGS fitting, while the second segment (between 10 and 15 seconds)

serves as novel view data, simulating the experience of driving into the future. Partitioning the novel frames based on their timestamps into five temporal buckets allows a systematic evaluation of NVS performance over increasing temporal distances from the reference views. Notably, the final bucket (14–15s) presents a significantly more challenging scenario due to accumulated floater artifacts, scene changes, and occlusions.

**DL3DV data** To complement the driving datasets, we include the DL3DV-10K dataset [13], which features both bounded and unbounded scenes. This dataset enables further evaluation of NVS methods and comparison with the 3DGS-Enhancer [14], reported under three levels of view sparsity (3, 6, and 12 views). We follow the same experimental setup and train/test splits as used in 3DGS-Enhancer,

Method	PSNR↑	SSIM↑	LPIPS↓
OmniRe [5]	17.15	0.645	0.448
DIFIX3D [24]	17.12	0.612	0.371
DIFIX3D++ [20]	18.74	0.696	0.375
ViewMorpher3D	21.58	0.716	0.303

Table 3. **NVS image quality on nuScenes** Results of overall performance on extrapolated trajectories (up to 5 seconds).

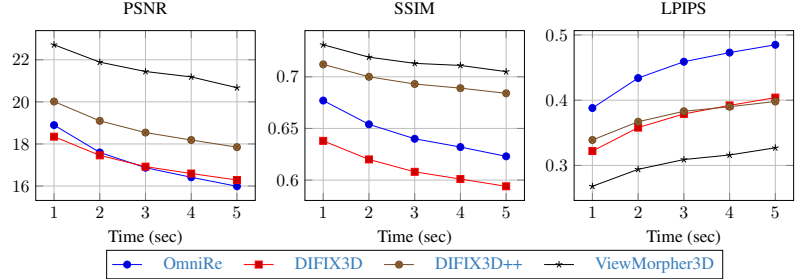


Figure 4. **NVS image quality under various signal-to-noise ratios on nuScenes**; The metrics for the extrapolated driving sequences (up to 5 seconds) are shown.



Figure 5. **Novel-view images of nuScenes**; (odd rows) a single reference camera image and rendered extrapolated views from 3DGS-based OmniRe model, up to 5 seconds; (even rows) enhanced images, conditioned on the given single reference view, using ViewMorpher3D.

conducting experiments on 130 training and 20 test scenes.

#### 4.2. Evaluation metrics

We evaluate the quality of synthesized novel-view images using PSNR, SSIM, and LPIPS metrics. These metrics are computed using ground-truth novel views provided by the datasets, and are sensitive to 3D consistency, view alignment, photometric fidelity and perceptual similarity.

#### 4.3. Implementation details

During training, each iteration processes a packet containing  $N + M$  frames, which includes a mix of reference and distorted target views. In our experiments, the packet size varies between 8 and 12 views per epoch. The ratio of reference to target views is flexible; however, each training packet is guaranteed to contain at least one reference view and one target view.

To select the most relevant reference views for the target views, we compute a view overlap score between every pair of reference and target cameras. Based on these scores, the top- $N$  reference views are selected for each packet. Further

details regarding the selection procedure are provided in the supplementary materials.

#### 4.4. Novel-view Enhancement Results

**EUVS Results** Table 1 reports performance of 3D reconstruction baselines and diffusion-based enhancers on 3DGS-rendered images. Across all EUVS novel-view settings, *ViewMorpher3D* consistently improves image quality and realism, outperforming state-of-the-art methods. Visual examples in Figure 3 show enhanced fidelity and restoration of distorted views compared to competing techniques.

**Para-Lane Results** Table 2 shows results on Para-Lane data. Our method achieves superior performance for single- and double-lane shifts, reducing LPIPS by about 50% relative to raw 3DGS images. Qualitative examples in Figure 3 confirm sharper details and restored content across challenging cross-lane viewpoints.

**nuScenes Results** Table 3 summarizes NVS performance using six nuScenes cameras over 5-second extrapolated sequences generated by OmniRe [5]. *ViewMorpher3D*



Figure 6. **Multi-camera enhancement** of extrapolated views from nuScenes.

Method	3 views			6 views			9 views		
	PSNR↑	SSIM↑	LPIPS↓	PSNR↑	SSIM↑	LPIPS↓	PSNR↑	SSIM↑	LPIPS↓
3DGS [11]	10.97	0.248	0.567	13.34	0.332	0.498	14.99	0.403	0.446
Mip-NeRF [1]	10.92	0.191	0.618	11.56	0.199	0.608	12.42	0.218	0.600
RegNeRF [19]	11.46	0.214	0.600	12.69	0.236	0.579	12.33	0.219	0.598
FreeNeRF [30]	10.91	0.211	0.595	12.13	0.230	0.576	12.85	0.241	0.573
DNGaussian [25]	11.10	0.273	0.579	12.67	0.329	0.547	13.44	0.365	0.539
DiFix3D [24]	14.90	0.460	0.338	16.90	0.527	0.266	17.86	0.560	0.235
3DGS-Enhancer [14]	14.33	0.424	0.464	16.94	0.565	0.356	18.50	<b>0.630</b>	0.305
DiFix3D++ [20]	15.93	0.528	0.361	17.95	<b>0.589</b>	0.291	18.93	0.619	0.262
ViewMorpher3D	<b>16.87</b>	<b>0.533</b>	<b>0.335</b>	<b>18.74</b>	0.587	<b>0.264</b>	<b>19.60</b>	0.614	<b>0.232</b>

Table 4. A quantitative comparison of few-shot 3D reconstruction. Experiments on DL3DV follow the data setting of [14]. The ViewMorpher3D is applied on 3DGS rendered images (appeared with gray color)

significantly improves image quality by correcting distortions. Metrics across temporal buckets in Figure 4 reveal lower SNR for longer extrapolations, which also is visually evident in degraded views in Figure 5. Plots highlight

our method’s superior fidelity and realism in restoring missing information, even under challenging temporal extrapolations.

**DL3DV Results** Table 4 reports NVS performance for



Figure 7. **NVS from DL3DV dataset**; (1<sup>st</sup> row) rendered images from sparse-view 3DGS fitting; (2<sup>nd</sup> row) DiFiX3D enhancement, given the closest trained view as reference; (3<sup>rd</sup> row) ViewMorpher3D enhancement using the same reference view as provided to DiFiX3D.

three sparse-view setups on DL3DV. All diffusion-based enhancers outperform 3DGS, with *ViewMorpher3D* achieving the best results across configurations, surpassing DiFiX3D and 3DGS-Enhancer. Notably, 3DGS-Enhancer uses iterative feedback of enhanced views into 3DGS optimization, whereas other methods—including ours—operate purely as post-processing without modifying geometry. This underscores *ViewMorpher3D*’s effectiveness in improving perceptual quality without retraining or iterative refinement.

#### 4.5. Ablation study

Table 5 presents the ablation study on some components of *ViewMorpher3D*.

Ablation	Configuration	PSNR	SSIM	LPIPS
Priors	w/o cond.	17.585	0.164	0.278
	w/o cameras	18.392	0.557	0.282
	w/o C-maps	18.428	0.560	0.288
	full	<b>18.739</b>	<b>0.587</b>	<b>0.265</b>
Architecture	w/o LoRA	18.604	0.584	0.287
	cross-attn	18.673	0.587	0.268

Table 5. **Ablation study** on the impact of 3D priors, fine-tuning VAE decoder and an alternative cross-attention modules on DL3DV (sparse 6 views)

**3D Priors:** We assess the contribution of 3D conditioning signals by selectively removing camera pose conditioning, 3D correspondence maps (C-maps), or both. The results show that excluding all conditioning (“w/o cond.”) leads to the lowest performance across all metrics. Conditioning on either camera Plücker rays or C-maps individually yields comparable improvements, while their combination (“full”) provides the best overall performance, indicating that these priors complement each other in guiding the synthesis process.

**Architecture:** We evaluated two architectural variants: removing LoRA-based fine-tuning of the VAE decoder (“w/o LoRA”) and replacing self-attention with cross-attention in the 2D UNet (“cross-attn”). LoRA fine-tuning slightly improves perceptual quality (LPIPS), suggesting enhanced realism in generated views. The cross-attention variant performs comparable to the baseline, indicating that it is a viable alternative for integrating latent priors.

## 5. Conclusion

In this work, we introduced *ViewMorpher3D*, a novel multi-camera diffusion model, designed to enhance novel view synthesis in autonomous driving scenarios. By leveraging a variable number of reference views and integrating 3D geometric priors and camera pose representations, *ViewMorpher3D* achieves high-fidelity restoration of target views with improved spatial and temporal consistency. Its flexible architecture allows it to adapt to diverse camera configurations across datasets and platforms, making it a versatile solution for real-world applications.

Our experimental results demonstrate that *ViewMorpher3D* sets a new benchmark in extrapolated novel-view synthesis across multiple driving datasets. The model’s ability to generate photorealistic and coherent views highlights its potential for integration into closed-loop simulation environments, where accurate visual feedback is critical. These contributions pave the way for more robust perception and planning systems in autonomous driving, and open avenues for future research in multi-view generative modeling and simulation-driven training.

## References

[1] Jonathan T Barron, Ben Mildenhall, Daniel Verbin, Pratul P Srinivasan, and Peter Hedman. Mip-nerf: A multiscale representation for anti-aliasing neural radiance fields. In *ICCV*, 2021. 7

[2] Jonathan T Barron, Ben Mildenhall, Dor Verbin, Pratul P Srinivasan, and Peter Hedman. Zip-nerf: Anti-aliased grid-based neural radiance fields. In *Proceedings of the IEEE/CVF International Conference on Computer Vision*, pages 19697–19705, 2023. 5

[3] Holger Caesar, Varun Bankiti, Alex H Lang, Sourabh Vora, Venice Erin Liang, Qiang Xu, Anush Krishnan, Yu Pan, Giancarlo Baldan, and Oscar Beijbom. nuscenes: A multi-modal dataset for autonomous driving. In *Proceedings of the IEEE/CVF conference on computer vision and pattern recognition*, pages 11621–11631, 2020. 4

[4] Danpeng Chen, Hai Li, Weicai Ye, Yifan Wang, Weijian Xie, Shangjin Zhai, Nan Wang, Haomin Liu, Hujun Bao, and Guofeng Zhang. Pgsr: Planar-based gaussian splatting for efficient and high-fidelity surface reconstruction. *IEEE Transactions on Visualization and Computer Graphics*, 2024. 5

[5] Ziyu Chen, Jiawei Yang, Jiahui Huang, Riccardo de Lutio, Janick Martinez Esturo, Boris Ivanovic, Ori Litany, Zan Gajcic, Sanja Fidler, Marco Pavone, Li Song, and Yue Wang. Omnire: Omni urban scene reconstruction. In *The Thirteenth International Conference on Learning Representations*, 2025. 2, 6

[6] Kai Cheng, Xiaoxiao Long, Kaizhi Yang, Yao Yao, Wei Yin, Yuexin Ma, Wenping Wang, and Xuejin Chen. Gaussianpro: 3d gaussian splatting with progressive propagation. In *Forty-first International Conference on Machine Learning*, 2024. 5

[7] Xiangyu Han, Zhen Jia, Boyi Li, Yan Wang, Boris Ivanovic, Yurong You, Lingjie Liu, Yue Wang, Marco Pavone, Chen Feng, et al. Extrapolated urban view synthesis benchmark. In *Proceedings of the IEEE/CVF International Conference on Computer Vision*, pages 28718–28728, 2025. 4, 11

[8] Binbin Huang, Zehao Yu, Anpei Chen, Andreas Geiger, and Shenghua Gao. 2d gaussian splatting for geometrically accurate radiance fields. In *ACM SIGGRAPH 2024 conference papers*, pages 1–11, 2024. 5

[9] Sungwon Hwang, Min-Jung Kim, Taewoong Kang, Jayeon Kang, and Jaegul Choo. Vefs: View extrapolation of urban scenes in 3d gaussian splatting using learned priors. In *European Conference on Computer Vision*, pages 1–18. Springer, 2024. 1, 2, 5

[10] Ajay Jain, Matthew Tancik, and Pieter Abbeel. Putting nerf on a diet: Semantically consistent few-shot view synthesis. In *Proceedings of the IEEE/CVF international conference on computer vision*, pages 5885–5894, 2021. 2

[11] Bernhard Kerbl, Georgios Kopanas, Thomas Leimkühler, and George Drettakis. 3d gaussian splatting for real-time radiance field rendering. *ACM Transactions on Graphics (TOG)*, 2023. 1, 2, 5, 7

[12] Yiming Li, Zehong Wang, Yue Wang, Zhiding Yu, Zan Gajcic, Marco Pavone, Chen Feng, and Jose M Alvarez. Memorize what matters: Emergent scene decomposition from multiview. *Advances in Neural Information Processing Systems*, 37:108389–108438, 2024. 5

[13] Lu Ling, Yichen Sheng, Zhi Tu, Wentian Zhao, Cheng Xin, Kun Wan, Lantao Yu, Qianyu Guo, Zixun Yu, Yawen Lu, et al. DL3dv-10k: A large-scale scene dataset for deep learning-based 3d vision. In *Proceedings of the IEEE/CVF Conference on Computer Vision and Pattern Recognition*, pages 22160–22169, 2024. 5

[14] Xi Liu, Chaoyi Zhou, and Siyu Huang. 3dgs-enhancer: Enhancing unbounded 3d gaussian splatting with view-consistent 2d diffusion priors. *Advances in Neural Information Processing Systems*, 37:133305–133327, 2024. 2, 5, 7

[15] Tao Lu, Mulin Yu, Lining Xu, Yuanbo Xiangli, Limin Wang, Dahua Lin, and Bo Dai. Scaffold-gs: Structured 3d gaussians for view-adaptive rendering. In *Proceedings of the IEEE/CVF Conference on Computer Vision and Pattern Recognition*, pages 20654–20664, 2024. 5

[16] Ben Mildenhall, Matthew Tancik, Pratul P Srinivasan, Jonathan T Barron, Ravi Ramamoorthi, and Ren Ng. Nerf: Representing scenes as neural radiance fields for view synthesis. In *ECCV*, 2020. 1, 2

[17] Thomas Müller, Alex Evans, Christoph Schied, and Alexander Keller. Instant neural graphics primitives with a multiresolution hash encoding. In *SIGGRAPH*, 2022. 5

[18] Ziqian Ni, Sicong Du, Zhenghua Hou, Chenming Wu, and Sheng Yang. Para-lane: Multi-lane dataset registering parallel scans for benchmarking novel view synthesis. *arXiv preprint arXiv:2502.15635*, 2025. 4

[19] Michael Niemeyer, Jonathan T Barron, Ben Mildenhall, et al. Regnerf: Regularizing neural radiance fields for few-shot novel view synthesis. In *CVPR*, 2022. 1, 2, 7

[20] Mohamed Omran, Farhad Zanjani, Davide Abati, Jens Petersen, and Amirhossein Habibian. Hybrid gaussian splatting for novel urban view synthesis. *arXiv preprint arXiv:2510.12308*, 2025. 2, 5, 6, 7

[21] Gaurav Parmar, Taesung Park, Srinivasa Narasimhan, and Jun-Yan Zhu. One-step image translation with text-to-image models. *arXiv preprint arXiv:2403.12036*, 2024. 4

[22] Tim Salimans and Jonathan Ho. Progressive distillation for fast sampling of diffusion models. *arXiv preprint arXiv:2202.00512*, 2022. 4

[23] Axel Sauer, Dominik Lorenz, Andreas Blattmann, and Robin Rombach. Adversarial diffusion distillation. In *European Conference on Computer Vision*, pages 87–103. Springer, 2024. 3

[24] Jay Zhangjie Wu, Yuxuan Zhang, Haithem Turki, Xuanchi Ren, Jun Gao, Mike Zheng Shou, Sanja Fidler, Zan Gajcic, and Huan Ling. Difix3d+: Improving 3d reconstructions with single-step diffusion models. *CVPR*, 2025. 2, 3, 4, 5, 6, 7, 11

[25] Jay Zhangjie Wu et al. Dngaussian: Depth-normal regularized gaussian splatting for improved 3d reconstruction. In *CVPR*, 2023. 1, 7

[26] Rundi Wu, Ben Mildenhall, Philipp Henzler, Keunhong Park, Ruiqi Gao, Daniel Watson, Pratul P Srinivasan, Dor Verbin, Jonathan T Barron, Ben Poole, et al. Reconfusion: 3d reconstruction with diffusion priors. In *Proceedings of*

*the IEEE/CVF conference on computer vision and pattern recognition*, pages 21551–21561, 2024. [2](#)

- [27] Zirui Wu, Tianyu Liu, Liyi Luo, Zhide Zhong, Jianteng Chen, Hongmin Xiao, Chao Hou, Haozhe Lou, Yuantao Chen, Runyi Yang, et al. Mars: An instance-aware, modular and realistic simulator for autonomous driving. In *CAAI International Conference on Artificial Intelligence*, pages 3–15. Springer, 2023. [2](#)
- [28] Yinghao Xu, Hao Tan, Fujun Luan, Sai Bi, Peng Wang, Jiahao Li, Zifan Shi, Kalyan Sunkavalli, Gordon Wetzstein, Zexiang Xu, et al. Dmv3d: Denoising multi-view diffusion using 3d large reconstruction model. *arXiv preprint arXiv:2311.09217*, 2023. [3](#)
- [29] Yunzhi Yan, Haotong Lin, Chenxu Zhou, Weijie Wang, Haiyang Sun, Kun Zhan, Xianpeng Lang, Xiaowei Zhou, and Sida Peng. Street gaussians: Modeling dynamic urban scenes with gaussian splatting. In *European Conference on Computer Vision*, pages 156–173. Springer, 2024. [2](#), [5](#)
- [30] Alex Yu, Zexiang Ye, Matthew Tancik, and Angjoo Kanazawa. Freenerf: Improving few-shot neural rendering with free viewpoint priors. In *CVPR*, 2021. [7](#)
- [31] Hongyu Zhou, Longzhong Lin, Jiabao Wang, Yichong Lu, Dongfeng Bai, Bingbing Liu, Yue Wang, Andreas Geiger, and Yiyi Liao. Hugsim: A real-time, photo-realistic and closed-loop simulator for autonomous driving. *arXiv preprint arXiv:2412.01718*, 2024. [2](#)
- [32] Shijie Zhou, Haoran Chang, Sicheng Jiang, Zhiwen Fan, Zehao Zhu, Dejia Xu, Pradyumna Chari, Suya You, Zhangyang Wang, and Achuta Kadambi. Feature 3dgs: Supercharging 3d gaussian splatting to enable distilled feature fields. In *Proceedings of the IEEE/CVF Conference on Computer Vision and Pattern Recognition*, pages 21676–21685, 2024. [5](#)
- [33] Xiaoyu Zhou, Zhiwei Lin, Xiaojun Shan, Yongtao Wang, Deqing Sun, and Ming-Hsuan Yang. Drivinggaussian: Composite gaussian splatting for surrounding dynamic autonomous driving scenes. In *Proceedings of the IEEE/CVF conference on computer vision and pattern recognition*, pages 21634–21643, 2024. [2](#)

# ViewMorpher3D: A 3D-Aware Diffusion Framework for Multi-Camera Novel View Synthesis in Autonomous Driving

## — Supplementary Material —

### A.1. Impact of Reference/Target View Count.

As mentioned earlier, *ViewMorpher3D* is trained on sampled packets of frames combining reference and target views. To understand the effect of varying the number of reference and target views, we conduct experiments on the DL3DV dataset. Results are summarized in Table 6.

We observe that increasing the number of reference views significantly improves image quality across all metrics. For example, moving from one reference view (Exp. 1) to three reference views (Exp. 3) yields a PSNR gain of over 1.1 dB and a noticeable improvement in SSIM and LPIPS. This suggests that additional reference views provide richer geometric and appearance cues for the diffusion process. Increasing the number of target views also leads to slight improvements, as rendered target views may contain complementary visual content that enhances consistency during image restoration. The best performance is achieved when both reference and target views are increased (Exp. 4), indicating that a balanced configuration benefits the model most.

Experiments	Configuration		PSNR	SSIM	LPIPS
	# Reference views	# Target views			
Exp. 1	1	2	17.58	0.556	0.279
Exp. 2	1	7	17.85	0.566	0.283
Exp. 3	3	2	18.69	0.588	<b>0.258</b>
Exp. 4	3	7	<b>18.80</b>	<b>0.592</b>	0.268

Table 6. **Effect of reference and target-Views count:** Increasing the number of reference views has a substantial impact on enhancement quality, while adding more target views provides marginal but consistent improvements. The combination of multiple reference and target views achieves the best overall performance, highlighting the importance of leveraging multi-view diffusion.

### A.2. Implementation Details

**Training Configuration.** The proposed *ViewMorpher3D* framework is trained on packets consisting of  $N + M$  frames, where  $N$  denotes reference views and  $M$  denotes target views. For the EUVS, Para-Lane, and DL3DV datasets, the packet length is fixed at 8. For nuScenes, which includes 6 cameras, the packet length is set to 12 (i.e., 6 reference and 6 target views). For inference, the packet length is increased to 16 for EUVS, Para-Lane, and DL3DV, and to 24 for nuScenes. Training is performed on 4 NVIDIA A100-80G GPUs with a total batch size of 4 for approximately 40K iterations.

During classifier-free guidance (CFG) training, we apply a dropout rate of 15% to both the C-map and camera pose. At inference time, the CFG scale is set to 2.0. All experiments are conducted at a resolution of  $576 \times 1024$  pixels. Following DiFix3D [24], we fine-tune SD-Turbo by introducing a lower noise level ( $\tau = 200$  instead of  $\tau = 1000$ ) rather than applying random Gaussian noise.

Consistent with prior work [7], for EUVS and Para-Lane, we utilize dynamic masks provided by the datasets to exclude pixels corresponding to potentially movable objects during both training and evaluation. These regions are also omitted during the initialization of 3DGS. This strategy addresses the fact that training and evaluation sequences often correspond to different traversals of the same scene, which may contain varying dynamic objects (e.g., vehicles, pedestrians). For nuScenes, dynamic objects are retained during both training and evaluation.

**Reference View Selection.** To select the most relevant reference views for the target views, we compute a *view overlap score* between each reference and target camera:

$$\text{score} = \alpha \cdot \frac{v_i \cdot v_j}{\|v_i\| \cdot \|v_j\|} + \beta \cdot \left(1 - \frac{d(c_i, c_j)}{\max_{i,j} d(c_i, c_j)}\right), \quad (5)$$

where  $v_i$  and  $v_j$  denote the view directions of the  $i^{\text{th}}$  and  $j^{\text{th}}$  cameras, respectively, and  $d(c_i, c_j)$  is the Euclidean distance between their camera centers, normalized by the maximum pairwise distance in the scene. The parameters  $\alpha$  and  $\beta$  control the relative importance of view alignment and spatial proximity. In all experiments, we set  $\alpha = 0.8$  and  $\beta = 0.2$ .

**3D Priors** For each packet, all camera poses and corresponding C-maps are transformed from world coordinates into the coordinate system of the first target camera. Before computing Plücker ray embeddings, we normalize the camera poses. This step is essential because the cross-product term  $\mathbf{o} \times \mathbf{d}$  is not scale-invariant, as it depends on the magnitude of  $\mathbf{o}$ . Furthermore, camera poses derived from Structure-from-Motion (SfM) often exhibit scale variations across different scenes or datasets. To address this issue, we normalize camera positions during both training and inference. Specifically, we scale the camera positions such that the maximum pairwise distance among all selected cameras within a training sample is set to unity. This normalization mitigates scale inconsistencies and promotes stable training across diverse scenes.

Camera poses and C-maps provide complementary 3D priors that guide the diffusion process. Figure 8 and Figure 9 illustrate visual examples of rendered RGB and C-maps from 3DGS.



Figure 8. Illustration of rendered 3DGS RGB images and corresponding coordinate maps (C-maps) from DL3DV scenes. Columns 1–3 depict reference views, while columns 4–6 show target views. The C-maps encode occlusion-aware 3D correspondences between views, where colors represent spatial consistency across different perspectives of the scene.



Figure 9. Example of 3DGS rendered RGB and coordinate maps (C-maps) from Para-Lane scene.